



1 **Variation in CO₂ and CH₄ Fluxes Among Land Cover Types in Heterogeneous Arctic Tundra**
2 **in Northeastern Siberia**

3

4 Sari Juutinen^{1,2}, Mika Aurela¹, Juha-Pekka Tuovinen¹, Viktor Ivakhov³, Maiju Linkosalmi¹, Aleksii
5 Räsänen^{4,5}, Tarmo Virtanen⁴, Juha Mikola^{4,5}, Johanna Nyman¹, Emmi Vähä¹, Marina Loskutova⁶,
6 Alexander Makshtas⁶, and Tuomas Laurila¹

7 1) Finnish Meteorological Institute, Erik Palménin aukio 1, 00560 Helsinki, Finland

8 2) Department of Geographical and Historical Studies, University of Eastern Finland,
9 Yliopistokatu 2, FI-80100 Joensuu, Finland (P.O. Box 111, FI-80101 Joensuu, Finland)

10 3) Voeikov Main Geophysical Observatory, Ulitsa Karbysheva, 7, St Petersburg, 194021,
11 Russia

12 4) Ecosystems and Environment Research Programme, University of Helsinki, Viikinkaari 1,
13 00790 Helsinki, Finland

14 5) Natural Resources Institute Finland (LUKE), Latokartanonkaari 9,
15 00790 Helsinki, Finland

16 6) Arctic and Antarctic Research Institute, Bering str., 38, St Petersburg, 199397, Russia

17

18

19 Corresponding author Sari Juutinen, sari.juutinen@uef.fi

20

21

22

23

24

25

26



27 **Abstract**

28 Arctic tundra is facing unprecedented warming, resulting in shifts in the vegetation, thaw regimes,
29 and potentially in the ecosystem-atmosphere exchange of carbon (C). The estimates of regional
30 carbon dioxide (CO₂) and methane (CH₄) budgets, however, are highly uncertain. We measured
31 CO₂ and CH₄ fluxes, vegetation composition and leaf area index (LAI), thaw depth, and soil
32 wetness in Tiksi (71° N, 128° E), a heterogeneous site located within the prostrate dwarf-shrub
33 tundra zone in northeastern Siberia. Using the closed chamber method, we determined net
34 ecosystem exchange (NEE) of CO₂, dark ecosystem respiration (ER), ecosystem gross
35 photosynthesis (Pg), and CH₄ fluxes during the growing season. We applied a previously developed
36 high-spatial-resolution land-cover map over an area of 35.8 km². Among the land-cover types
37 varying from barrens to dwarf-shrub tundra and tundra wetlands, the light-saturated NEE and Pg
38 scaled with the LAI of vascular plants. Thus, the graminoid-dominated tundra wetlands, with high
39 LAI and the deepest thaw depth, had the highest light-saturated NEE and Pg (up to -21 (uptake) and
40 28 mmol m⁻²h⁻¹, respectively) and were disproportionately important for the summertime CO₂
41 sequestration on a landscape scale. Dry tundra, including the dwarf-shrub-dominated vegetation and
42 only sparsely vegetated lichen tundra, had only small CO₂ exchange rates. While tundra wetlands
43 were sources of CH₄, lichen tundra, including bare ground habitats, consumed atmospheric CH₄ at a
44 substantial rate. On a landscape scale, the consumption by lichen tundra and barrens could offset *ca.*
45 10% of the CH₄ emissions. We acknowledge the uncertainty involved in spatial extrapolations due
46 to a small number of replicates per land-cover type. This study, however, highlights the need for
47 distinguishing different land-cover types including the dry tundra habitats to account for their
48 consumption of the atmospheric CH₄ when estimating tundra C-exchange on a larger spatial scale.

49

50

51



52 **1 Introduction**

53 It is uncertain whether the Arctic tundra is a sink or a source of atmospheric carbon (C). The current
54 estimates suggest a sink of 13–110 Tg C yr⁻¹, but their uncertainty range crosses the zero balance
55 (McGuire et al. 2012, Virkkala et al. 2020). Improving these estimates is vital, because the Arctic
56 tundra covers a vast area of 7.6 million km² (Walker 2000) that is experiencing substantial warming
57 (IPCC 2013, Chen et al. 2021). Warming can alter C exchange, either amplifying or mitigating
58 climate change through ecosystem–atmosphere interactions. Some local-scale studies suggest that
59 the Arctic tundra is shifting from a small sink to a source of C (Webb et al. 2016, Euskirchen et al.
60 2017). It is likely that the climate change response of the ecosystem carbon dioxide (CO₂) sink
61 strength and methane (CH₄) emissions, whether an increase or a decrease, depends on site-specific
62 changes in thawing, wetness, and vegetation (McGuire et al. 2018). C dynamics of different tundra
63 habitats need to be quantified across the Arctic to improve the upscaling of arctic CO₂ and CH₄
64 balances and to monitor how ecosystems respond to environmental changes.

65 The uncertainty in the arctic C balance estimates arises from the sparse and uneven
66 observation network, which provides poor support for model-based spatial extrapolation (*cf.*
67 McGuire et al. 2018, Virkkala et al. 2021). On a local scale, landscape heterogeneity and the related
68 difficulty of mapping the spatial distribution of habitats and their C fluxes add to this uncertainty
69 (McGuire et al. 2012, Treat et al. 2018, Saunois et al. 2020). In addition, year-to-year variations in
70 seasonal features, particularly the timing of spring, summer temperatures, and snow depth have
71 been found to cause substantial variation in the annual net CO₂ and CH₄ balances (Aurela et al.
72 2004, Humphreys and Lafleur 2011, Zhang et al. 2019).

73 Fine-scale spatial heterogeneity in soil water saturation, thaw depth, vegetation
74 characteristics, and soil organic content is typical of the tundra landscape (*e.g.*, Virtanen and Ek
75 2014, Mikola et al. 2018, Lara et al. 2020). These factors control CO₂ and CH₄ exchange, and on an
76 annual scale, tundra wetlands typically act as net CO₂ sinks while upland tundra areas have a close-



77 to-neutral C balance (*e.g.*, Marushchak et al. 2013, Virkkala et al. 2021). While tundra wetlands are
78 substantial sources of CH₄, dry tundra act as a small sink of atmospheric CH₄. Particularly, the
79 tundra barrens show high consumption rates of atmospheric CH₄ due to the high-affinity methane
80 oxidizing bacteria (Jørgensen et al. 2014, Lau et al. 2015, D’Imperio et al. 2017, Oh et al. 2020).
81 Thus, distinguishing dry and wet tundra with their moisture and vegetation characteristics is crucial
82 when mapping C exchange within the tundra biome. Treat et al. (2018) tested spatial resolution
83 requirements for such mapping on a landscape level and found that a 20-m pixel size captured the
84 spatial variation in a reasonable manner, while a coarser resolution resulted in underestimation of
85 both the landscape-scale CO₂ uptake and CH₄ emissions. In addition, understanding the spatial
86 heterogeneity of ecosystem C exchange substantially enhances analyses of micrometeorological
87 measurements that, while in principle representing spatially integrated fluxes, may provide biased
88 balances in a highly heterogeneous environment (*e.g.*, Tuovinen et al. 2019). Thus, plot-scale data,
89 allowing studies of the local relationship between gas exchange and soil and vegetation properties,
90 are necessary for improving and validating upscaling methods.

91 The aim of this study was to assess the spatial patterns and magnitudes of CO₂ and
92 CH₄ fluxes within heterogenous prostrate dwarf-shrub tundra in Tiksi, located in northeastern
93 Russia. Growing season fluxes of CO₂ (ecosystem net exchange, photosynthesis, and respiration)
94 and CH₄ were determined using the chamber method to answer the questions: (i) what is the
95 magnitude of these fluxes in different land-cover types? And (ii) how do they depend on vegetation
96 characteristics and soil wetness? In addition, to test the spatial representativeness of the chamber
97 data, we extrapolated the habitat-level measurements in space to compare them with the ecosystem-
98 level data measured with the micrometeorological eddy covariance (EC) technique.

99
100
101



102 **2 Materials and Methods**

103 *2.1 Study site*

104 The study site is located near the Tiksi Observatory (see Uttal et al. 2016) in Yakutia, northeastern
105 Russia (71.5943 N, 128.8878 E), 500 m inland off the Laptev Sea coast and, on average, 7 m above
106 sea level (Fig. 1). The area belongs to the middle-arctic prostrate dwarf-shrub tundra subzone
107 (Walker, 2000) and has continuous permafrost. In the end of the growing season, the maximum
108 thaw depth is 40 cm (Mikola et al. 2018). Climate in Tiksi is defined by cold winters and cool
109 summers. The long-term mean annual temperature and mean annual precipitation were -12.7 °C and
110 232 mm, respectively, during the normal period 1981–2010. Growing season lasts about 3 months,
111 and the soils typically freeze in the end of September and the permanent snow falls in October and
112 thaws in June (AARI 2018).

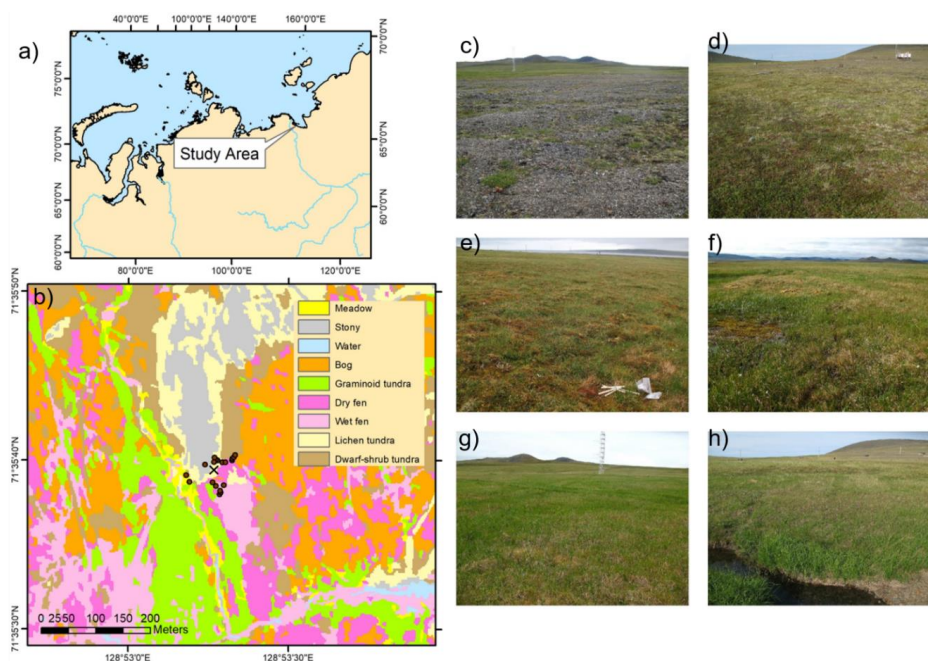
113 Soil organic content varies from negligible in lichen covered and bare graveled areas
114 to *ca.* 40% in tundra wetlands (Mikola et al. 2018). Bedrock and soils are alkaline, resulting in high
115 plant species richness. Vegetation consists of mosses, lichens, grasses, sedges, prostrate dwarf-
116 shrubs such as willows (*Salix* spp.), dwarf birch (*Betula nana*), and *Diapensia lapponica*, and forb
117 species (Fig. 1, Table 1). The average heights of dwarf-shrub species are 4–6 cm and the leaf area
118 index (LAI) of vascular plants reaches up to 1 m² m⁻² in the wetland and meadow habitats with
119 graminoid vegetation (Juutinen et al. 2017). The land cover at the site has been classified *a priori*
120 and mapped based on a combination of field inventories and high-spatial resolution satellite images
121 (Mikola et al. 2018). The *a priori* land-cover types (LCT) consist of wet fen, dry fen, graminoid
122 tundra, bog, meadow at the stream bank, dwarf-shrub tundra, and lichen tundra (includes bare
123 ground with vegetation patches) (Table 1). A section of the wet and dry fen within the EC footprint
124 area is disturbed by vehicle tracks that create open water surfaces, and there is also an area of
125 eroded bare-peat surface on a dry fen.

126



127

128



129

130 **Fig. 1.** a) Location of the study area in Tiksi, Yakutia, Russia, b) Land-cover map and the chamber
131 flux measurement points (dots) and the EC mast (x) on the map, and photos of the LC types: c)
132 lichen tundra with barrens, lichens, and patches of vegetation, d) dwarf-shrub tundra, e) bog, f) wet
133 and dry fen, g) graminoid tundra, and h) meadow by the stream.

134

135

136

137

138

139

140

141

142



143 **Table 1.** Soil and vegetation characteristics of the land cover types (LCT) and their proportions in
 144 the EC impact area (90% of the cumulative footprint).

LCT	Soil properties and plant taxa	Proportion (%) ²
Lichen tundra ¹	Mixture of vegetated patches, stones, and bare ground. Lichens, <i>Dryas octopetala</i> , <i>Vaccinium vitis-idaea</i> , <i>Salix polaris</i> , <i>Diapensia lapponica</i> , <i>Oxytropis</i> spp, <i>Astragalus</i> spp., <i>Pedicularis</i> spp., <i>Artemisia</i> spp., <i>Minuartia</i> sp.,	8 (barren), 11 (sparse vegetation)
Dwarf-shrub tundra	Shallow organic layer on mineral soil ground Feather mosses, lichens, <i>Salix polaris</i> , <i>Vaccinium vitis-idaea</i> , <i>Vaccinium uliginosum</i> , <i>Dryas octopetala</i> , <i>Cassiope tetragona</i> , <i>Betula nana</i> , <i>Polygonum viviparum</i> , <i>Pedicularis</i> spp., <i>Carex</i> spp.	18
Meadow	Shallow organic layer on mineral soil ground <i>Calamagrostis</i> sp., <i>Festuca</i> sp, <i>Salix</i> spp. <i>Polygonum viviparum</i> , <i>Bistorta major</i> , <i>Polemonium</i> sp., <i>Valeriana</i> sp.	1.4
Graminoid tundra	Shallow peat layer on mineral soil ground Feather mosses, <i>Sphagnum</i> spp., <i>Carex</i> spp., <i>Eriophorum</i> spp., <i>Calamagrostis</i> spp., <i>Salix</i> spp., <i>B. nana</i> , <i>Saxifraga</i> spp., <i>Ranunculus</i> spp., <i>Bistorta major</i> , <i>Stellaria</i> sp., <i>Valeriana</i> sp., <i>Polemonium</i> sp., <i>Comarum palustre</i>	13
Bog	Dry hummock habitat at the tundra peatland <i>Sphagnum</i> spp., feather mosses, <i>Salix</i> spp., <i>Vaccinium uliginosum</i> , <i>Vaccinium vitis-idaea</i> , <i>Betula nana</i> , <i>Rhodendron tomentosum</i> , <i>Cassiope tetragona</i> , <i>Carex</i> spp., <i>Polygonum viviparum</i> ., <i>Stellaria</i> sp.	23
Dry fen	Intermediate wet tundra peatland habitat <i>Sphagnum</i> spp., <i>Carex</i> spp., <i>Salix</i> spp, <i>Saxifraga</i> spp., <i>Comarum palustre</i> , <i>Epilobium</i> spp., <i>Ranunculus</i> spp., <i>Pedicularis</i> spp., <i>Stellaria</i> sp.	10
Wet fen	Wet tundra peatland habitat with open pools <i>Brown mosses</i> , <i>Carex</i> spp., <i>Eriophorum</i> spp., <i>Ranunculus</i> sp., <i>Caltha palustris</i> , <i>Pedicularis</i> sp., <i>Saxifraga</i> sp.	15

145 ¹⁾ Combined land-cover types bare and lichen tundra in Juutinen et al. (2017), Mikola et al. (2018),
 146 Tuovinen et al. (2019), ²⁾ Proportion within the 90% coverage of the mean EC footprint area during
 147 the growing season of 2014 (Tuovinen et al. 2019).

148
 149
 150
 151



152 *2.2 CO₂ and CH₄ flux measurements*

153 Fluxes of CO₂ and CH₄ were measured using static chambers set on 12 pre-installed collars of 50
 154 cm × 50 cm. The measurement points (collars) were set to cover the heterogeneity in land cover,
 155 and in each study year, there were 1–4 measurement points per each LCT (Table 2). Most of the
 156 data were collected during a study campaign in July 15 – August 16, 2014. The growing season had
 157 started earlier due to a warm period and daily mean air temperature stayed over 5 °C since July 5
 158 (Fig. 2) (Tuovinen et al. 2019). Net ecosystem exchange of CO₂ (NEE) and ecosystem respiration
 159 of CO₂ in dark (ER) were measured using transparent and opaque chambers (transparent chamber
 160 covered with a hood), respectively, allowing the estimation of ecosystem gross photosynthesis (Pg)
 161 as difference of NEE and ER. Fluxes of CH₄ were determined from closures of both transparent and
 162 opaque chambers, but because there was no difference between them when performed
 163 consecutively, the data from transparent chamber measurements were used for flux calculations. In
 164 addition, CH₄ fluxes were measured during shorter campaigns in 2012, 2013, 2016, and 2019
 165 (Table 2). These data also included vehicle track disturbance plots and an eroded bare-peat surface,
 166 which were measured in 2019.

167 **Table 2.** Measurement periods, measured fluxes (CH₄, ER, NEE), and number of measurement
 168 points and observations (points, observations) in each land cover type (LCT) across the study years.

LCT	2012	2013	2014	2016	2019
	Jul 18–21	Jul 5–Sep 3	Jul 15–Aug 16	May 30, Aug 4–5, Sep 13–14	Aug 28–Sep 1
	CH ₄	CH ₄	ER, NEE, CH ₄	CH ₄	CH ₄
Wet fen	4, 4	6, 22	3, 107	3, 27	5, 72
Vehicle track					2, 30
Dry fen	2, 2	4, 11	3, 107	3, 14	2, 26
Bare peat					1, 15
Bog	2, 2	3, 7	1, 36		1, 13
Meadow	1, 1	2, 6	2, 62		
Dwarf-shrub tundra	1, 1		1, 36	1, 1	
Lichen tundra		1, 3	2, 67	2, 18	2, 29
Snow and ice ¹				2, 2	

¹Measured only on May 30, 2016.



169 In 2012 and 2013, CH₄ concentrations inside the chamber were analyzed from
170 samples stored in glass vials using a gas chromatograph equipped with a flame ionization detector
171 in the laboratory of the Voeikov Main Geophysical Observatory. Four samples per each 20-min
172 chamber closure were collected. Since July 2014, CH₄ and CO₂ concentrations inside the chambers
173 were recorded every second during closures of about 5-min using a gas analyzer (Los Gatos
174 Research, DLT-100). Gas fluxes between the ecosystem and the atmosphere were calculated from
175 the phase of linear concentration change in the chamber head space over time accounting for
176 temperature, volume, and atmospheric pressure. Concentration change during each chamber closure
177 was evaluated visually for determining the closure start time and to remove cases showing
178 nonlinearity due to leaks, ebullition, or saturation. There were a few ebullition cases at the vehicle
179 track measurement points that had only sparse or no vegetation cover.

180 The fluxes of CO₂ and CH₄ were also measured by the micrometeorological EC
181 method, which provides continuous data of the atmosphere-biosphere fluxes averaged on an
182 ecosystem scale. The EC system consisted of a three-dimensional sonic anemometer (USA-1,
183 METEK GmbH, Elmshorn, Germany), a closed-path CH₄ analyzer (RMT-200, LGR, Inc., CA,
184 USA), and a closed-path CO₂/H₂O analyzer (LI-COR LI-7000, Inc., Lincoln, NE, USA). The fluxes
185 were calculated as 30-min averages and processed using standard methods (Aubinet et al. 2012).
186 The EC measurement system and the post-processing procedures have been presented in more
187 detail by Tuovinen et al. (2019).

188 Supporting meteorological measurements including air temperature (T_{air}) (Vaisala,
189 HMP), soil temperature (T_{soil}) (IKES, Nokeval), photosynthetic photon flux density (PPFD) (Kipp
190 & Zonen, PQS1), and water table level relative to the ground surface (WT) (8438.66.2646, Trafag)
191 were collected by a Vaisala QML datalogger as 30-min averages. We also present meteorological
192 data for the period 2011–2019 to relate the conditions during the measurement campaign in Jul 15-



193 Aug 16, 2014, and the CH₄ flux campaigns in 2012, 2013, 2014, 2016, and 2019, to the nine-year
194 overall.

195

196 2.3 Vegetation and Topographic Wetness Index

197 On a site level, vegetation and soil characteristics were inventoried in plots assigned into a
198 systematic grid outside the area covered by the gas flux measurement points in 2014 (see Juutinen
199 et al. 2017; Mikola et al. 2018). The projection cover (%) of plant species and species groups, and
200 the mean canopy height of each species group were recorded. Seven species groups were included
201 in the inventory: *Sphagnum* mosses, feather mosses, brown mosses, dwarf shrubs, *Betula nana*,
202 *Salix* species, forbs, and graminoids. A subset of the plots was harvested, and vascular plant leaves
203 were scanned to determine the one-sided LAI to estimate empirical relationships between LAI and
204 %-cover and canopy height to estimate LAI in the collars (see Juutinen et al. 2017). In the collars,
205 cover (%) and height (cm) of each species group were recorded weekly during the gas flux
206 measurement campaign July 15–August 16, 2014. Because there were no observational vegetation
207 data for the other years than 2014, the green chromatic coordinate (GCC) was used as a proxy for
208 the amount of green above-ground vascular plants (*e.g.* Richardson 2019). GCC was calculated
209 from the digital numbers of red (R), green (G), and blue (B) color channels as the ratio of green in
210 the images ($GCC = G / (R + G + B)$) from digital RGB photos of the vegetation inside the collars. The
211 photos were taken at the time of measurements. We determined an empirical relationship between
212 LAI and GCC by using a data set of harvested plots with digital RGB photographs and measured
213 LAI data (n=91). Data distributions varied among the LCTs due to the intrinsic differences and
214 amount of vegetation. For the LAI estimation, we used a linear relationship ($R^2 = 0.46$, $p < 0.001$)
215 between LAI and GCC determined using the entire data set (see appendix Fig. 1 for the data and
216 equation).



217 To quantify potential soil wetness at each measurement point, we calculated the mean
218 topographic wetness index (TWI) value based on a 2 m spatial resolution digital elevation model
219 (Mikola et al. 2018). To characterize differences between growing seasons as manifested by
220 vegetation greenness, MODIS Normalized Difference Vegetation Index (NDVI) with 16-day
221 temporal and 500 m spatial resolution was calculated for a circular area with 300 m radius from the
222 flux tower using Google Earth Engine (Gorelick et al. 2017). NDVI was derived for 2011–2019 to
223 place the measurement years in the context of year-to-year variation in weather.

224

225 2.4 Data analyses

226 When examining the role of the habitat types in CO₂ and CH₄ exchange, we applied the land cover
227 classification presented in Mikola et al. (2018). The data collected in July 15 – August 16, 2014
228 were used for examining gas exchange in relation to the variation in LAI, GCC, WT, and TWI
229 among the collars. Utilizing the ER and NEE fluxes measured with opaque and transparent
230 chambers, respectively, we assessed the light response of P_g and NEE with a hyperbolic function

231

$$232 \text{NEE} = \text{ER} - P_{g_{\max}} \times \text{PPFD} / (\beta + \text{PPFD}), \quad \text{eq. 1.}$$

233

234

235 where $P_{g_{\max}}$ is the asymptotic maximum of photosynthesis, and β is the half-saturation PPFD. To
236 ensure comparability between different measurement days in relatively low light conditions, we
237 determined the light-normalized $P_{g_{800}}$, *i.e.*, P_g at PPFD = 800 $\mu\text{mol m}^{-2} \text{s}^{-1}$. The corresponding
238 NEE, *i.e.*, NEE_{800} , is then obtained as a sum of $P_{g_{800}}$ and ER. Fluxes of CH₄ are expressed as collar
239 means. We used a sign convention where a positive value means net release to the atmosphere and a
240 negative value denotes net uptake by the ecosystem.

241 To find the main factors and gradients in the plant community, gas flux, and
242 environmental variables data measured in the flux collars in 2014, we performed a detrended
243 correspondence analysis (DCA) of the species group data with post-hoc fit of environmental



244 variables, including gas fluxes, WT, LAI, GCC, elevation, and thaw depth as supplementary
245 variables. The DCA was performed on logarithmically transformed, centered species data (species
246 as species groups) using Canoco 5 (Ter Braak and Šmilauer 2012). Regression analyses were used
247 to test the relationships between gas flux estimates and vascular LAI, GCC, WT, and TWI. All CH₄
248 flux data from the years 2012–14, 2016, and 2019 were used to quantify the mean growing season
249 CH₄ flux for each LCT and examine the relationship between CH₄ and GCC and TWI.

250 We compared the LCT-specific flux estimates based on the chamber measurements
251 with the estimates based on EC measurements over the same period. Partitioning of the EC-based
252 CO₂ fluxes to Pg and ER and estimates of Pg₈₀₀ and NEE₈₀₀ were calculated similarly to that of
253 chamber data using Eq. (1). The EC flux data were classified into five wind sectors (30–125°, 125–
254 185°, 185–239°, 239–310°, 310–360° based on the mean EC flux footprint, modeled for the
255 growing of 2014 by Tuovinen et al. (2019). The sectors distinguished areas dominated by different
256 LCTs, especially tundra heaths and wetlands, and, similarly, sectors with large and small vascular
257 LAI. For each sector, the footprint-weighted areal proportions of LCTs and mean vascular LAI
258 were derived from the high spatial resolution land-cover and LAI maps (Mikola et al. 2018). For
259 this comparison, sector averages of Pg₈₀₀, ER, NEE₈₀₀, and CH₄ flux were calculated from the
260 chamber data by weighting the LCT-specific flux estimates with the above-mentioned LCT
261 proportions in each sector. Because there were no measurement points within graminoid tundra, we
262 applied wet fen (for CO₂) and dry fen (for CH₄) flux estimates for the graminoid tundra based on
263 the observed similarities in LAI and soil wetness, respectively. Overall, graminoid tundra can be
264 considered part of the fen continuum in terms of soil characteristics (high organic content) and CH₄
265 exchange (Mikola et al. 2018, Tuovinen et al. 2019).

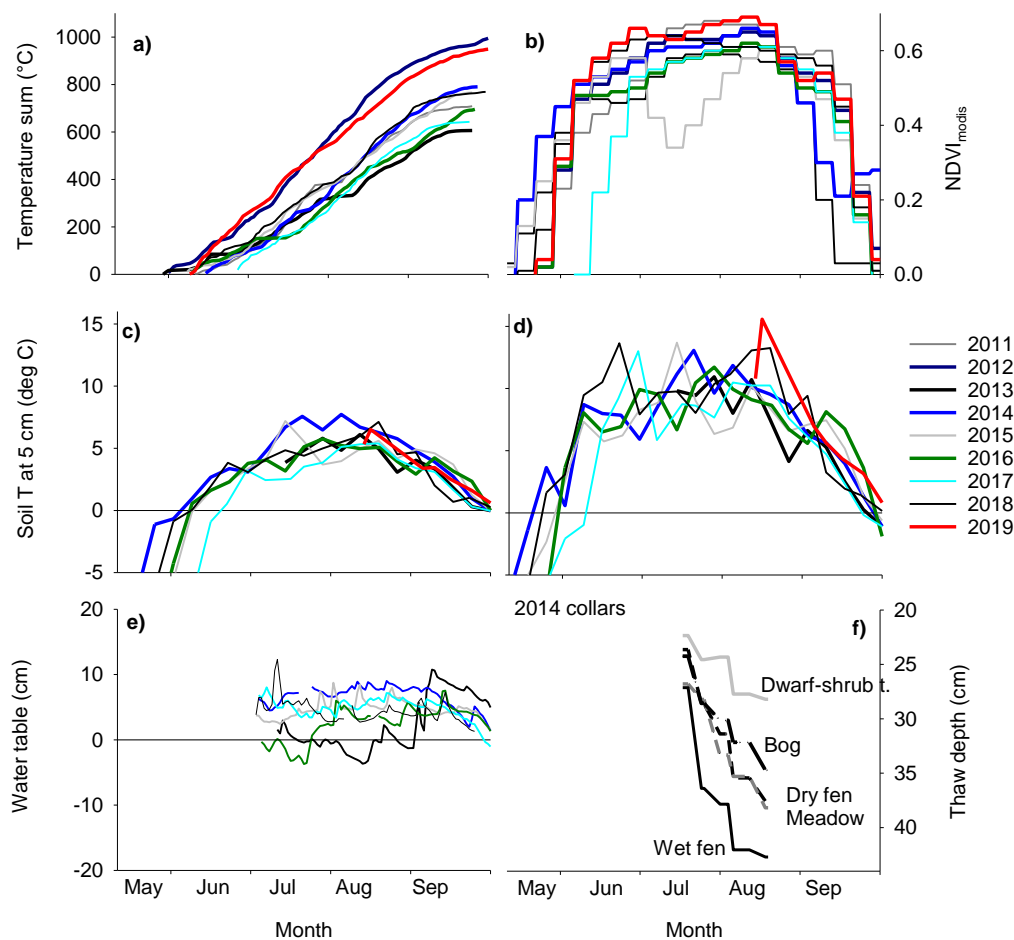
266 Finally, to synthesize the CO₂ and CH₄ exchange variability across the tundra, we
267 upscaled the LCT-specific average NEE₈₀₀, Pg₈₀₀, ER, and CH₄ flux to the 35.8 km² area
268 surrounding our study site, for which a LCT map was produced by Mikola et al. (2018).



269 **3 Results**

270 *3.1 Meteorology*

271 In 2014, when we collected most of the flux data, temperature sum accumulation (with a 0 °C T_{air}
272 threshold) was near-average during the thaw period (the period when soil surface temperature was
273 continuously above 0°C), but the spring and mid-growing season were warmer than on average
274 (Fig. 2a). The average air temperature was 15°C during the gas flux measurements. Accordingly,
275 the MODIS NDVI showed an early start of greening (Fig. 2b-d), and vegetation development had
276 already started at the beginning of the measurement period. In 2010–2019, which included the other
277 CH₄ measurement years, the thaw period lasted for 74–124 days, creating a temperature sum range
278 of 642–1003 °C days (Fig. 2a). Surface soils thawed between May 28 and July 9 and froze again
279 between September 21 and October 1. Among the observation years, the years 2012 and 2019 had
280 notably longer and warmer thaw periods than the other years. The driest habitat, lichen tundra,
281 thawed 10–15 days earlier than the other habitats, and had ca. 3 °C higher soil temperature than the
282 wet fen at the depth of 5 cm (Fig. 2b–c). Water table depth, measured at a wet fen location, showed
283 only subtle interannual variation (Fig. 2e). In 2014, the active layer depth, measured over the
284 measurement period close to the collars, was deepest in the end of August, reaching 30–40 cm in
285 the wetland and meadow habitats, and remained < 30 cm in the dry dwarf-shrub tundra (Fig. 2f).
286 Lichen tundra had rocks underneath the loose surface layer, which made it impossible to measure
287 the actual thaw depth.



288

289

290 **Fig. 2.** Meteorology in May to September in years 2011–2019. **(a)** Air temperature accumulation
291 with threshold values soil surface $> 0\text{ }^{\circ}\text{C}$ and air $T > 0\text{ }^{\circ}\text{C}$, **(b)** seasonal dynamics of NDVI in the
292 study area, 16 d aggregated MODIS data, **(c)** weekly means of soil temperature at depth of 5 cm in
293 wet fen and **(d)** in dry tundra, **(e)** water table relative to the ground surface in wet fen, and **(f)** LCT
294 means of thaw depth in the measurement collars in 2014.

295

296 3.2 Multivariate analysis

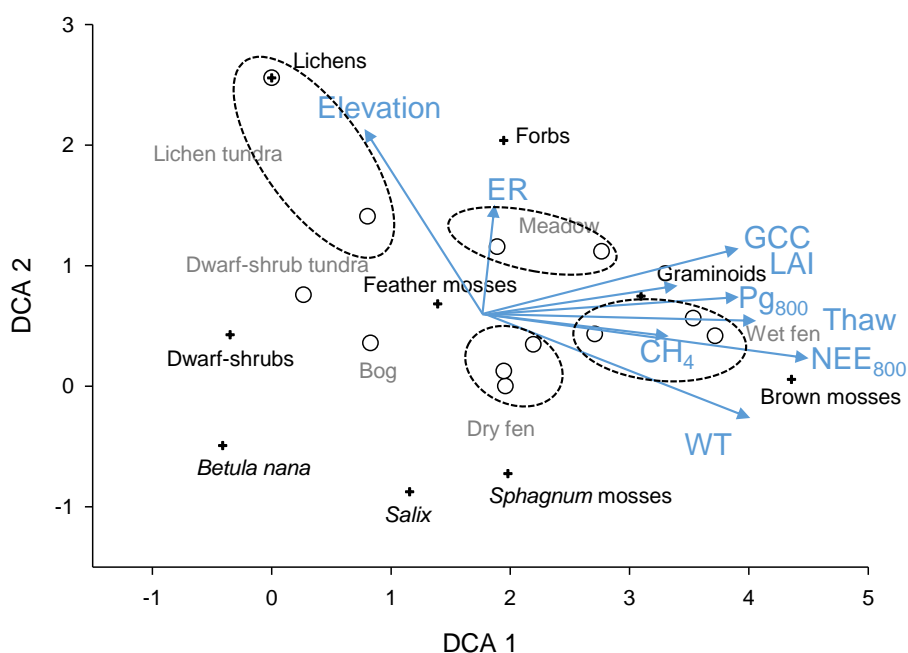
297 DCA axes 1 and 2, which explained 49% and 14% of the variation in the grouped species data (Fig.

298 3). Lichen tundra and wet fen plots differed most from each other along the axis 1. Accordingly, the

299 supplementary variables WT, vascular plant LAI, thaw depth, TWI, GCC, Pg_{800} , NEE_{800} , and CH_4



300 fluxes correlated positively with the axis 1 with post-hoc correlations (r) of 0.6–0.9, as derived from
301 the DCA weighted correlation matrix. Elevation had a positive correlation with the axis 2 ($r = 0.8$),
302 along which there were gradients in moss abundance and soil organic content.
303
304



305
306

307 **Fig. 3.** DCA ordination diagram based on species (species groups) data from the measurement
308 collars in 2014. In the plot, the scores of species groups (cross), sample plots (open symbols), and
309 post-hoc fits of supplementary variables (arrows, blue type) mean CH_4 , Pg_{800} , ER, NEE_{800} , thaw
310 depth (Thaw), water table relative to the ground surface (WT), green chromatic coordinate (GCC),
311 vascular plant LAI, and elevation above sea level (Elevation). Land-cover types of the sample plots
312 are indicated (grey type) and plots assigned to same LCTs are circled. Eigenvalues for axis 1 and 2
313 are 0.597 and 0.171, respectively, and axis 1 and 2 explain cumulatively 63% of the variation in the
314 species group data.

315

316 3.3 Exchange of CO_2 and CH_4

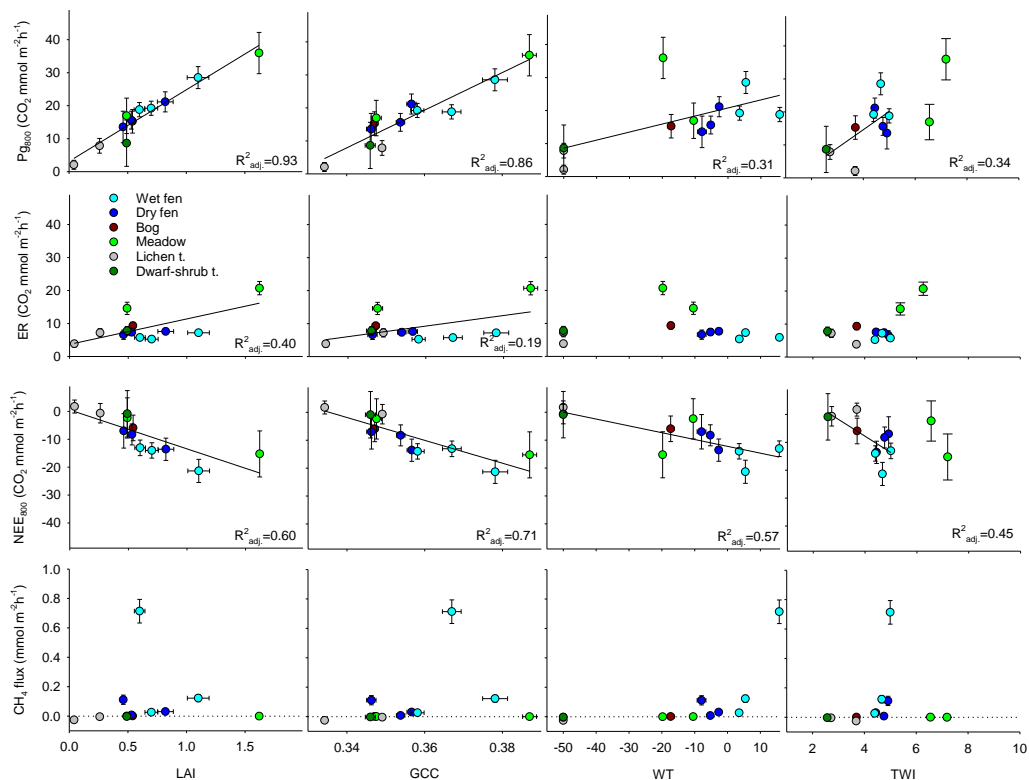
317 Among different LCTs, the light-normalized photosynthesis (Pg_{800}) varied from about 5 mmol m^{-2}
318 h^{-1} in the lichen tundra to about 22 and $27 \text{ mmol m}^{-2} \text{ h}^{-1}$ in the wet fen and meadow, respectively.



319 P_{g800} was strongly and positively related to the vascular plant LAI and the greenness index GCC
320 (Fig. 4). There was also a positive correlation between P_{g800} and WT and TWI, possibly because the
321 highest LAI occurred at the wet fen and meadow plots. However, the TWI values for the two
322 meadow plots located on an elevated bank of the stream were disproportionately high in relation to
323 the WT at the plots, probably because of insufficient locational accuracy or an artefact in the digital
324 elevation model. Ecosystem respiration was higher in the two meadow plots, on average 18 mmol
325 $m^{-2}h^{-1}$ than in other plots. The relationship between ER and LAI was weaker than that of P_{g800} and
326 LAI (Fig. 4). The net exchange, NEE_{800} , varied from about zero in the lichen tundra plots to a net
327 CO_2 uptake of 16 mmol $m^{-2}h^{-1}$ in the meadow and wet fen plots. NEE_{800} was more tightly linked to
328 P_{g800} than ER and was correlated with LAI, GCC, WT, and TWI (Fig. 4).

329 There was substantial consumption of the atmospheric CH_4 in the lichen tundra plots
330 (mean -0.02 mmol $m^{-2}h^{-1}$, Fig. 5). Minor consumption occurred in the meadow, dwarf-shrub tundra,
331 and bog plots (mean <-0.002 mmol $m^{-2}h^{-1}$), and efflux to the atmosphere was observed in the dry
332 fen and wet fen plots (means 0.05 and 0.16 mmol $m^{-2}h^{-1}$, respectively, Fig. 5). The eroded bare-peat
333 plot within the dry fen habitat and the vehicle-track plots in wet fen had large emissions (up to 0.2
334 mmol $m^{-2}h^{-1}$), which were of the same magnitude as in the undisturbed dry and wet fen habitats.
335 Variation among the plot means (Fig. 4, year 2014 data) was positively correlated with WT. Large
336 CH_4 emissions occurred when TWI was > 4 , except the two meadow plots, which showed net
337 consumption of CH_4 but had an unrealistically high TWI (see above and Figs. 4 and 6). Variation in
338 CH_4 fluxes was not related to variation in LAI or GCC.

339
340



341

342

343 **Fig. 4.** Variation in estimates of Pg_{800} , ER, NEE_{800} (Eq. 1) and collar means of CH_4 fluxes in
344 relation to variation in collar means of LAI, GCC, WT and TWI on July 6–August 16, 2014. Error
345 bars denote the standard error of estimate. Fitted regression lines and adjusted coefficients of
346 determination (R^2_{adj}) are included for significant linear relationships. The two meadow plots were
347 not included in the TWI regressions.

348

349

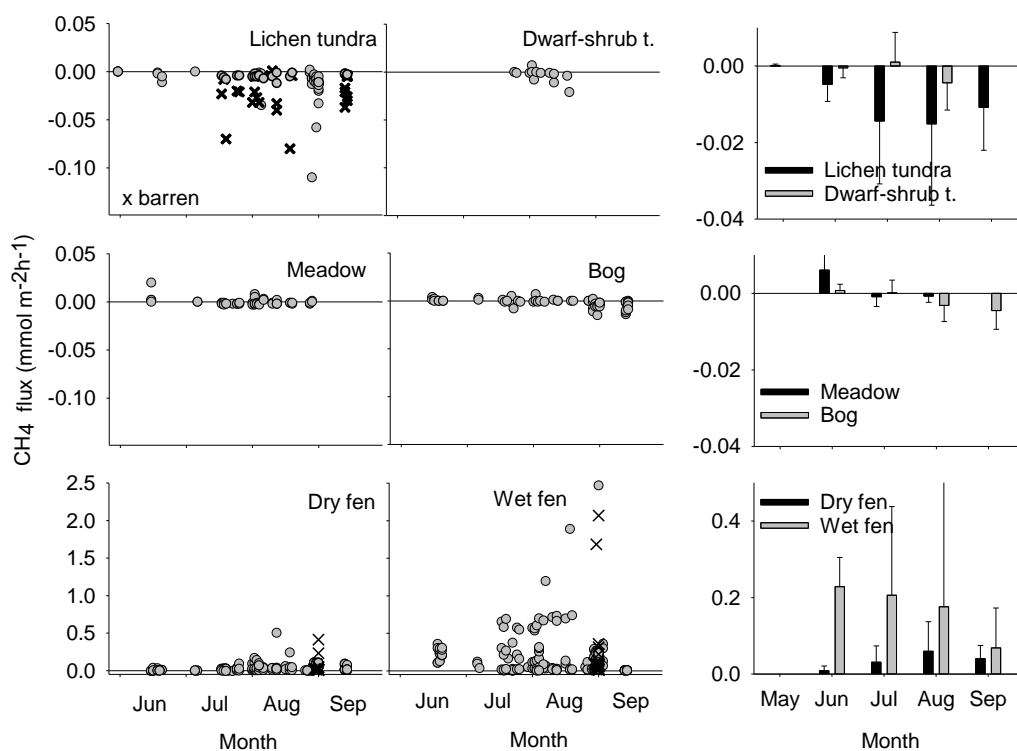
350

351

352

353

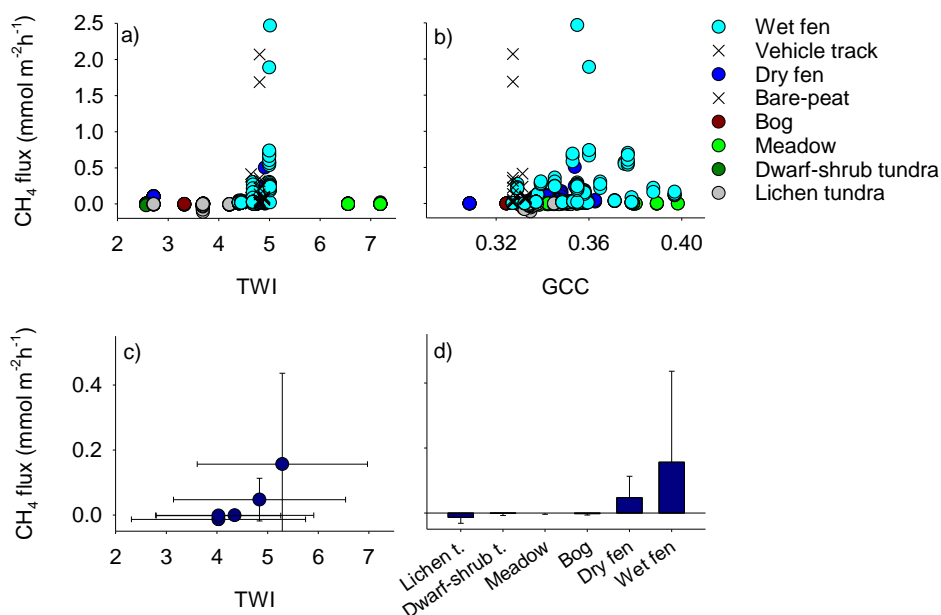
354



355

356 **Fig. 5.** Instantaneous (left panels) and monthly mean (right panels, with \pm SD error bars) CH₄ fluxes
357 in each LTC. The data are a composite of all study years. Barren surfaces are indicated among the
358 lichen tundra data. The eroded bare-peat and vehicle-track plots are plotted as part of the dry fen
359 and wet fen data (×), respectively, but these data are not included in the monthly means. Note that
360 the panel groups have different y-axis scales.

361



362

363 **Fig. 6.** Instantaneous CH₄ fluxes in the LCTs in relation to **a)** plot specific TWI and **b)** GCC and **c)**
364 LCT mean (±SD) CH₄ fluxes in relation to LCT mean (±SD) TWI (excluding the meadow plots
365 with erroneous TWI) and **d)** LCT mean CH₄ fluxes (±SD). Data from years 2014, 2016, and 2019.

366

367

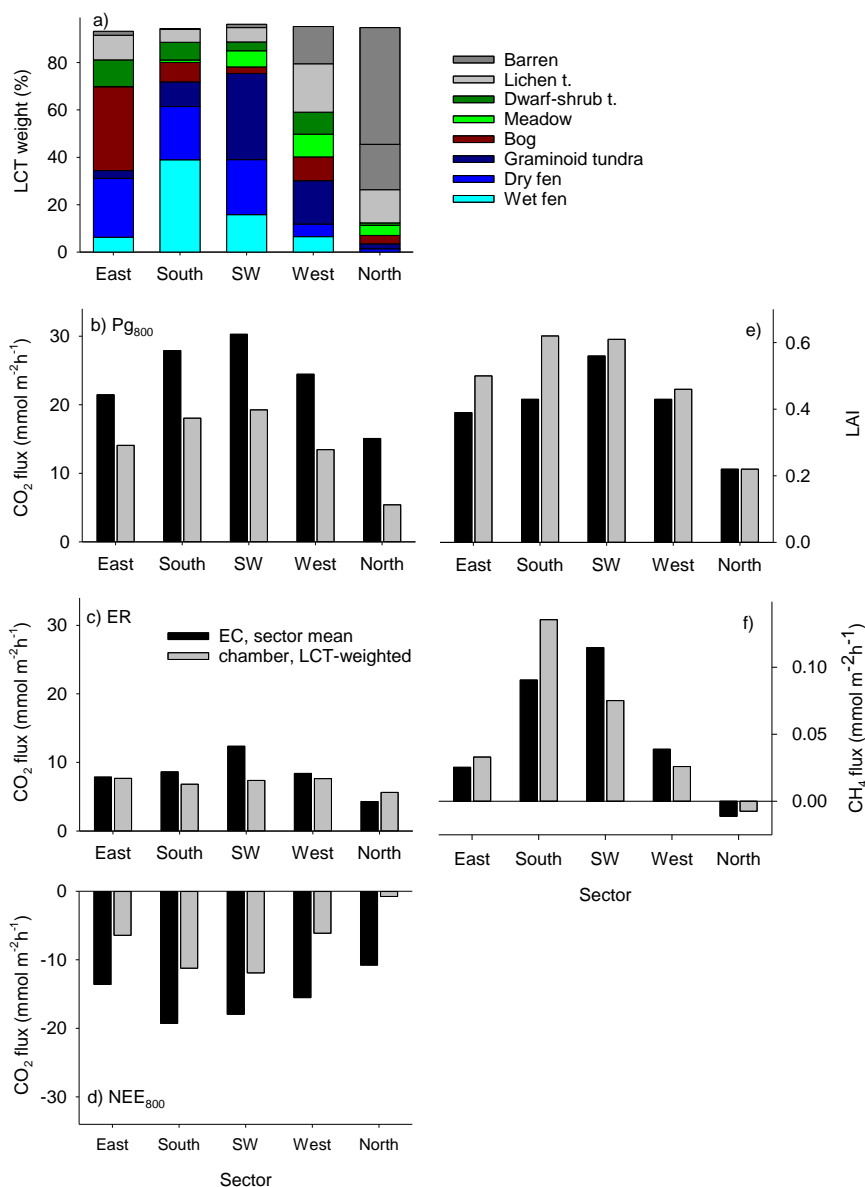
To compare the chamber-based flux data with those derived from the EC
368 measurements, the EC data were classified based on wind direction, which reflects the varying
369 domination of different LCTs within the EC source area. In both the southern and south-western
370 wind sectors (125–185° and 185–239°), wet fen and graminoid tundra together contributed *ca.* 40%
371 of the footprint-weighted LCT areas (Fig. 7a). In these directions, vegetation mainly consisted of
372 graminoids, as dry fen, wet fen, graminoid tundra, and meadow contributed 80% in total. The
373 northern sector (310–360°) was characterized by the abundance of lichen tundra and bare ground
374 that accounted for 68% of the footprint-weighted LCT areas, while all the other LCTs covered less
375 than 18% in total. The other wind direction sectors had more even LCT distributions. The
376 differences between the sectors were similar in the EC-based and spatially weighted chamber-based
377 averages of CO₂ exchange (Fig. 7). Both Pg₈₀₀ and NEE₈₀₀ were largest in the southern and south–



378 western sectors and clearly smallest in the barren–lichen tundra-dominated sector in the north. The
379 chamber-based estimates of CO₂ exchange were, however, lower: Pg₈₀₀ was 57%, ER was 93%, and
380 NEE₈₀₀ was 44% of the EC-based estimate.

381 The southern and south-western wind sectors with abundant dry and wet fens and
382 graminoid tundra had clearly the largest CH₄ fluxes (Fig. 7). The estimate based on chamber
383 measurements was 30% and 50% larger than the EC-based estimate for the east sector (dominated
384 by dry fen and bog) and south sector (dominated by dry and wet fen), respectively. In contrast, the
385 chamber-based estimate was 56–67% of the EC-based estimate for the other sectors, dominated by
386 graminoid tundra and lichen tundra.

387 Within the extended study area of 35.8 km², the LCT-weighted mean NEE₈₀₀,
388 corresponding to the LCT-specific chamber-based fluxes that were upscaled with the footprint-
389 weighted LCT areas, was -6 mmol m⁻² h⁻¹ (uptake relative to the atmosphere). The corresponding
390 mean Pg₈₀₀ was 12 mmol m⁻² h⁻¹, and CH₄ flux 0.05 mmol m⁻² h⁻¹ (Table 3). Relative to their spatial
391 cover (28% in total), wet and dry fens were disproportionally important for the landscape-level net
392 exchange of CO₂, photosynthesis, and CH₄, contributing 74%, 47%, and 99% of the net landscape
393 totals (Table 3). Consumption of CH₄ by lichen tundra (including barrens), dwarf-shrub tundra, and
394 meadow tundra soils was 10% of the CH₄ emission. Particularly, the barrens contributed to the
395 consumption of CH₄ due to their large area and high consumption rate. Note, however, that the EC-
396 based estimates for the wind direction sectors suggested about two times as high NEE₈₀₀ and *ca.*
397 30% smaller CH₄ emissions for the wet fens, and 30% larger consumption for the barrens and
398 lichen tundra.



399

400 **Fig. 7. a)** Footprint-weighted mean contribution of each LCT to the EC measurements divided into
 401 wind direction sectors, and comparison of EC and chamber-based sector means of **b-d)** CO_2
 402 exchange (P_{g800} , ER, and NEE_{800}) **e)** vascular plant LAI, and **f)** CH_4 fluxes. The chamber-based
 403 data are weighted by the LCT proportions shown in panel a. Map of LAI (Tuovinen et al., 2019)
 404 and the LAI measured in the collars were used to estimate the EC- and chamber-related sector
 405 means, respectively.

406

407



408 **Table 3.** Land-cover type distribution in the mapped 35.8 km² area, means and standard errors (se)
 409 calculated from the collar-specific estimates of Pg₈₀₀, ER, NEE₈₀₀ and CH₄ based on the 2014 data,
 410 and proportional (%) landscape budgets.

LCT	Area (%)	Pg ₈₀₀ (mmol m ⁻² h ⁻¹)		ER (mmol m ⁻² h ⁻¹)		NEE ₈₀₀ (mmol m ⁻² h ⁻¹)		CH ₄ flux (mmol m ⁻² h ⁻¹)		NEE ₈₀₀ (%)	Pg ₈₀₀ (%)	CH ₄ flux (%)
		mean	sd	mean	sd	mean	sd	mean	sd			
Mean ¹		11.21		6.60		-4.61		0.053				
Wet fen	16.4	21.93	-3.91	6.44	0.98	-15.49	3.39	0.223	0.286	55.1	32.1	88.66
Dry fen	11.6	14.60	1.02	6.99	0.39	-7.61	0.64	0.059	0.052	19.1	15.1	10.80
Gram. t.	3.4	21.93	3.91	6.44	0.98	-15.49	3.39	0.059	0.052	11.4	6.7	10.77
Bog	9.1	15.27		9.34		-5.93		0.000		11.7	12.4	0.03
Meadow	0.4	26.45	9.51	17.66	3.06	-8.79	6.45	-0.001	<0.001	0.8	0.9	-0.01
Dwarf-s. t.	27.4	8.64		7.80		-0.85		-0.003		5.0	21.1	-1.65
Lichen t.	11.1	4.98	2.87	5.53	1.68	0.55	1.20	-0.005		-1.3	4.9	-1.05
Barren	15.3	4.98	2.87	5.53	1.68	0.55	1.20	-0.026		-1.8	6.8	-7.56
Water	5.3	NA		NA		NA		NA				

411 ¹ Spatial LCT area-weighted mean, ² Graminoid tundra fluxes estimated using values for wet fen
 412 (CO₂) and dry fen (CH₄)

413
 414

415 **4 Discussion**

416 The studied tundra site in Tiksi in northeastern Siberia has heterogeneous land cover, which is
 417 reflected as equally heterogeneous CO₂ and CH₄ exchange. On the one hand, we found that the
 418 tundra wetlands have a disproportional role: dry and wet fens and meadow had the highest CO₂
 419 uptake capacity and particularly the wet fen showed high CH₄ emissions. On the other hand, our
 420 results highlight the high consumption of atmospheric CH₄ by lichen tundra (barrens and small
 421 vegetated patches). This CH₄ consumption is high compared to other non-wetland tundra habitats
 422 and, on the landscape scale, could offset 9 of the CH₄ emissions. These data augment the
 423 knowledge on the functional diversity, namely distribution of different land-cover types, and their
 424 emission factors across the vast arctic tundra and will lend support to bottom-up and top-down
 425 extrapolations across the Arctic.

426 Within this tundra landscape, the graminoid-dominated wetlands with organic-rich soils
 427 constitute an important part of the ecosystem-atmosphere exchange of CO₂ and CH₄. Within an area



428 of 35.8 km² mapped around our study site (Mikola et al. 2018), wet and dry fens and the fen-like
429 graminoid tundra covered 31% of the area but contributed as much as 73% to the potential light-
430 saturated CO₂ sink during the peak growing season. These wetlands are also the sites having high
431 soil organic matter content and C pools (Mikola et al. 2018) and CH₄ emissions to the atmosphere
432 (see also Tuovinen et al. 2019).

433 The spatial extrapolation of fluxes is clearly sensitive to a small number of chamber
434 measurement points as there is large within-LCT variation e.g., in the wet fen and meadow data. For
435 this reason, it is neither possible to conclude which LCTs differ significantly from each other in the
436 CO₂ or CH₄ fluxes. Our conclusions made from the chamber data are, however, corroborated by the
437 temporally matching section of EC data, categorized by wind direction to reflect the main LCT
438 patterns around the EC mast, which show similarity to the chamber data. Instead of categorical LCT
439 classification, maps of those variables, LAI, and WT, for instance, that drive CO₂ and CH₄
440 exchange would be preferable for spatial modeling of these ecosystem functions (Räsänen et al.
441 2021). Mikola et al. (2018) found, however, that distinguishing, for instance, soil organic content
442 based on remote sensing and using the same LCT classification was a challenge in the same site.

443 The spatial pattern of the growing season light-saturated photosynthesis and net CO₂
444 exchange was strongly related to the corresponding pattern of the LAI of vascular plants (Fig. 3, 4).
445 Hence, the abundance of graminoid (Cyperaceae and Poaceae) vegetation predicted a large NEE₈₀₀,
446 which varied from near zero in lichen tundra up to 25 mmol m⁻² h⁻¹ in wet fen. Ecosystem
447 respiration had a smaller role than Pg in determining NEE, but we note that our data cover only a
448 section of the growing season with warmer temperatures and half to full-grown vegetation. The
449 importance of ER is likely to be different when considering the full annual balance (e.g., Hashemi
450 et al. 2021). While our data represent only the growing season, a similar relationship has also been
451 found between the annual NEE and LAI at a tundra site with a mixture of wet and dry tundra in
452 northeastern Europe (Marushchak et al. 2013), in a multi-site EC study in Alaskan tundra



453 (McFadden et al. 2003), in Canadian low arctic tundra wetlands (Lafleur et al. 2012), and across
454 tundra sites (Street et al. 2007; Shaver et al. 2007).

455 The magnitude of P_{g800} and NEE_{800} in the fen and meadow plots of this study were
456 similar to the maximum P_g and NEE found in tundra wetland in Seida in northeastern Europe
457 (Marushchak et al. 2013), at low tundra wetland sites in eastern Canada (Lafleur et al. 2012), and at
458 a wetland-dominated but more continental site (with an equal growing season length) in
459 northeastern Siberia (van der Molen et al. 2007). The vegetation and P_{g800} of lichen tundra and
460 dwarf-shrub tundra in our study resembled those observed within the polygon rim habitat of the
461 polygon tundra in the Lena River delta, while those of meadow, dry fen, and wet fen resembled the
462 wet polygon center habitats (Eckhardt et al. 2019). In our study, the variation of ecosystem
463 respiration resulted from the variation in vascular plant LAI, soil organic content, and water
464 saturation: the highest ER occurred in mineral soil meadow with high LAI suggesting substantial
465 autotrophic respiration and likely deep rooting and large root biomass contributing to the ecosystem
466 respiration (Fig. 4). In wetlands, respiration may be attenuated by the soil water saturation.

467 Our chamber-based estimate of the average CH_4 flux within the 35.8 km² upscaling area
468 was 0.05 mmol m⁻² h⁻¹, which is close to 0.04 mmol m⁻² h⁻¹ obtained by Tuovinen et al. (2019) who
469 combined EC data with footprint modeling to statistically determine LCT group-specific CH_4
470 fluxes. Within this upscaling area, 28% of the area emitted CH_4 , while the other habitats either
471 consumed atmospheric CH_4 (lichen tundra including barrens, coverage 26%) or were close to
472 neutral relative to the atmosphere (Figs. 4, 5, Table 3). The wettest spots were the sites having the
473 highest CH_4 emissions (Fig. 4). We observed no clear relationship between vegetation and CH_4 flux
474 in plot level, which could partly be due to the small size of data. At a LCT level, high LAI and high
475 CH_4 emissions co-occurred if WT was high enough (Fig. 3). The sites showing the highest
476 emissions had a high soil organic matter content, an indication of slow decomposition in anoxic
477 conditions, and we also found that the eroded bare-peat surface of dry fen and the disturbed vehicle



478 tracks had high CH₄ emissions. In the case of eroding surfaces, gas efflux may be enhanced by
479 transport pathways emerging from changes in soil structure. Wet depressions, like the vehicle tracks
480 in this study, have in turn been found to have high CH₄ emissions relative to their surroundings in
481 permafrost, which results from the abundance of graminoids producing easily degradable litter
482 compared to dwarf-shrubs, and the potentially increasing nutrients from seasonal permafrost
483 degradation (*e.g.*, Bubier et al. 1995, McCalley et al. 2014, Wickland et al. 2020). All in all, our
484 data encourage applying indicators of wetness together with vegetation parameters as a means of
485 CH₄ flux upscaling in tundra environment. While the topographic wetness index in general was a
486 reasonable surrogate for WT, distinguishing the dry and wet soils, erroneous TWI values were
487 estimated for the streamside meadow, possibly due to insufficient locational accuracy, because the
488 plots were located right next to the stream, but on an elevated bank.

489 The recognition of CH₄ consuming tundra habitats is important for accurately estimating
490 the net CH₄ balance of tundra. The substantial uptake of atmospheric CH₄ by lichen tundra (here a
491 mixture of bare ground and sparse vegetation) in Tiksi was inferred by Tuovinen et al. (2019) based
492 on a source allocation analysis of EC data: the average flux of the consuming area was estimated at
493 -0.03 mmol m⁻² h⁻¹, which corresponds to -21.6% of the total upscaled CH₄ flux. In this study, the
494 average growing season CH₄ uptake was -0.02 mmol m⁻² h⁻¹ in the lichen tundra plots and an order
495 of magnitude lower in graminoid tundra, dwarf-shrub tundra, and bog. Our upscaling exercise
496 resulted in a CH₄ sink that counterbalanced about -10% of the CH₄ emission, which likely is an
497 underestimate due to an overestimation of the emissions from the wet fens. High consumption of
498 atmospheric CH₄ in barrens is associated with the high affinity methanotrophs (Jørgensen et al.
499 2014; Lau et al. 2015; D’Imperio et al. 2017, St Pierre et al. 2019). For instance, on Disko Island,
500 Greenland, which consists of similar land cover types to Tiksi, uptake of CH₄ by bare ground was -
501 0.005–0.01 mmol m⁻² h⁻¹ during the growing season, while a mean flux of -0.003–0.004 mmol m⁻²
502 h⁻¹ was observed in dry tundra heath (D’Imperio et al. 2017). These consumption rates associated



503 with tundra barrens and high-affinity methanotrophs can be high relative to consumption rates
504 measured on north-boreal forest soils (for instance, $-0.01 \text{ mmol m}^{-2}\text{h}^{-1}$, Lohila et al. 2016).

505

506 **5 Conclusions**

507 Our results provide new observations of carbon exchange for the prostrate dwarf shrub tundra sub-
508 zone, which covers an area of 2.3 million km^2 of the Arctic (Walker 2000). Graminoid vegetation
509 favored the wet and moist habitats, such as wet fens and the streamside meadow, which were
510 characterized by large CO_2 uptake and CH_4 emissions. The heterogeneity of landscape and the
511 related large spatial variability of CO_2 and CH_4 fluxes observed in this study encourage to monitor
512 the Arctic sites for changes in habitat type distribution. Such changes can include the forming of
513 meadows and appearance of new vegetation communities, such as erect shrubs, that benefit of
514 warming-induced changes in thaw depth and soil wetness. The spatial extrapolation based on a
515 small number of measurement points involves inherent uncertainty but still allowed us to identify
516 key relationships between CO_2 and CH_4 fluxes and vegetation and moisture features, which can be
517 utilized in more robust upscaling experiments that make use of EC measurements.

518

519 *Data availability.* The flux data used in this study can be accessed via the Zenodo data repository:
520 Juutinen, Sari. (2022). Dataset for a manuscript entitled Variation in CO_2 and CH_4 Fluxes Among
521 Land Cover Types in Heterogeneous Arctic Tundra in Northeastern Siberia [Data set]. Zenodo.

522 <https://doi.org/10.5281/zenodo.5825705>

523

524

525

526

527



528 *Author contributions*

529 TL, MA, and SJ designed the study. TL, MA, and AM took care of the overall site governance and
530 maintenance. VI, ML, TL, JM, JN, EV, TL, TV, and MA conceived the field measurements of CO₂
531 and CH₄, vegetation, and environmental variables. In addition, ML calculated green chromatic
532 coordinates, and MA and J-PT postprocessed the EC data and J-PT modeled the footprint and
533 estimated footprint LCT fractions. AR and TV processed and modelled the landcover data and
534 estimated TWI and NDVI for the plots and area. SJ compiled the chamber flux data and conducted
535 the data analyses and spatial extrapolations and wrote the manuscript with contributions from all co-
536 authors.

537

538 *Competing interests*

539 The authors declare that they have no conflict of interest.

540

541 *Acknowledgements*

542 We thank G. Chumachenko, O. Dmitrieva, and E. Volkov at the Tiksi Observatory and the
543 Yakutian Hydrometeorological Service for their kind assistance in carrying out and organizing the
544 field campaigns and Lauri Rosenius for assistance in the field work. This study was financially
545 supported by the Academy of Finland, projects “Greenhouse gas, aerosol and albedo variations in
546 the changing Arctic” (project no. 269095), “Carbon balance under changing processes of Arctic and
547 subarctic cryosphere” (project no. 285630), “Constraining uncertainties in the permafrost-climate
548 feedback” (project no. 291736) and “Carbon dynamics across Arctic landscape gradients: past,
549 present and future” (project no. 296888); the European Commission, FP7 project “Changing
550 permafrost in the Arctic and its global effects in the 21st century (PAGE21, project no. 282700”);
551 and the Nordic Council of Ministers, DEFROST Nordic Centre of Excellence within NordForsk.

552



553 **References**

- 554 AARI: Archive of Tiksi standard meteorological observations (1932–2016), Russian Federal
555 Service for Hydrometeorology and Environmental Monitoring, St Petersburg, Russia,
556 available at: http://www.aari.ru/resources/d0024/archive/description_e.html, last
557 access: 13 September 2018.
- 558 Aurela, M., Laurila, T., and Tuovinen, J-P.: The timing of snow melt controls the annual CO₂
559 balance in a subarctic fen, *Geophysical Research Letters* 31, L16119,
560 doi:10.1029/2004GL020315, 2004.
- 561 Bubier, J.L., Moore, T.R., Bellisario, L., Comer, N.T., and Crill, P.M: Ecological controls on
562 methane emissions from a northern peatland complex in the zone of discontinuous
563 permafrost, Manitoba, Canada. *Global Biogeochemical Cycles* 9. 455–470, 1995.
- 564 Chen, L., Aalto, J., and Luoto, M.: Significant shallow–depth soil warming over Russia during the
565 past 40 years. *Global and Planetary Change*, 197, 103394,
566 doi.org/10.1016/j.gloplacha.2020.103394, 2021.
- 567 D’Imperio, L., Skov Nielsen, C., Westergaard-Nielsen, A., Michelsen, A., and Elberling, B.:
568 Methane oxidation in contrasting soil types: responses to experimental warming with
569 implication for landscapeintegrated CH₄ budget. *Global Change Biology* 23, 966–
570 976, doi: 10.1111/gcb.13400, 2017.
- 571 Eckhardt, T., Knoblauch, C., Kutzbach, L., Holl, D., Simpson, G., Abakumov, E., and Pfeiffer, E-
572 M.: Partitioning net ecosystem exchange of CO₂ on the pedon scale in the Lena River
573 Delta, Siberia. *Biogeosciences* 16, 1543–1562, doi:10.5194/bg-16-1543-2019, 2019.
- 574 Euskirchen, E.S., Bret-Harte, M.S., Shaver, G.R., Edgar, C.W., and Romanovsky, V.E.: Long-Term
575 Release of Carbon Dioxide from Arctic Tundra Ecosystems in Alaska. *Ecosystems* 20,
576 960–974, doi: 10.1007/s10021-016-0085-9, 2017.



- 577 Gorelick, N., Hancher, M., Dixon, M., Ilyushchenko, S., Thau, D., and Moore, R.: Google Earth
578 Engine: Planetary-scale geospatial analysis for everyone. *Remote Sensing of*
579 *Environment*, 202, 18-27, doi.org/10.1016/j.rse.2017.06.031, 2017.
- 580 Hashemi, J., Zona, D., Arndt, K.A., Kalhori, A., and Oechel, W.C.: Seasonality buffers carbon
581 budget variability across heterogeneous landscapes in Alaskan Arctic Tundra.
582 *Environ. Res. Lett.* in press <https://doi.org/10.1088/1748-9326/abe2d1>, 2021.
- 583 Humphreys, E.R. and Lafleur, P.M.: Does earlier snowmelt lead to greater CO₂ sequestration in
584 two low Arctic tundra ecosystems? *Geophysical Research Letters* 38, L09703,
585 doi:10.1029/2011GL047339, 2011.
- 586 IPCC Summary for Policymakers in *Climate Change 2013: The Physical Science Basis* (eds
587 Stocker, T. F. et al.) 3–29, Cambridge Univ, Press, 2013.
- 588 Jørgensen, C.J., Lund Johansen, K.M., Westergaard-Nielsen, A., and Elberling, B.: Net regional
589 methane sink in High Arctic soils of northeast Greenland. *Nature Geoscience* 8, doi:
590 10.1038/NGEO2305, 2014.
- 591 Juutinen, S., Virtanen, T., Kondratyev, V., Laurila, T., Linkosalmi, M., Mikola, J., Nyman, J.,
592 Räsänen, A., Tuovinen, J-P., and Aurela, M.: Spatial variation and seasonal dynamics
593 of leaf-area index in the arctic tundra – implications for linking ground observations
594 and satellite images. *Environmental Research Letters* 12, doi.org/10.1088/1748-
595 9326/aa7f85, 2017.
- 596 Lau, M.C.Y., Stackhouse, B.T., Layton, A.C., Chauhan, A., Vishnivetskaya, T.A., Chourey, K.,
597 Ronholm, J., Mykityczuk, N.C.S., Bennett, P.C., Lamarche-Gagnon, G., Burton, N.,
598 Pollard, W.H., Omelon, C.R., Medvigy, D.M., Hettich, R.L., Pfiffner, S.M., Whyte,
599 L.G., and Onstott, T.C.: An active atmospheric methane sink in high Arctic mineral
600 cryosols. *The ISME Journal* 9, 1880–1891, doi:10.1038/ismej.2015.13, 2015.



- 601 Lafleur, P.M., Humphreys, E.R., St. Louis, V.L., Myklebust, M.C., Papakyriakou, T., Poissant, L.,
602 Barker, J.D., Pilote, M., and Swystun, K.A.: Variation in Peak Growing Season Net
603 Ecosystem Production Across the Canadian Arctic. *Environmental Science and*
604 *Technology* 46, 7971–7977, doi.org/10.1021/es300500m, 2012.
- 605 Lara, M.J., McGuire, A.D., Euskirchen, E.S., Genet H., Yi, S., Rutter, R., Iversen, C., Sloan, V.,
606 and Wullschleger, S.D.: Local-scale Arctic tundra heterogeneity affects regional-scale
607 carbon dynamics- *Nature Communications* 11, 4925, doi:10.1038/s41467-020-18768-
608 z, 2020.
- 609 Lohila, A., Aalto, T., Aurela, M., Hatakka, J., Tuovinen, J-P., Kilkki, J., Penttilä, T., Vuorenmaa, J.,
610 Hänninen, P., Sutinen, R., Viisanen, Y., and Laurila, T.: Large contribution of boreal
611 upland forest soils to a catchment-scale CH₄ balance in a wet year. *Geophysical*
612 *Research Letters* 43, 2946–2953, doi.org/10.1002/2016GL067718, 2016.
- 613 Marushchak, M.E., Kiepe, I., Biasi, C., Elsakov, V., Friborg, T., Johansson, T., Soegaard, H.,
614 Virtanen, T., and Martikainen, P.J.: Carbon dioxide balance of subarctic tundra from
615 plot to regional scales. *Biogeosciences* 10, 437–452, doi:10.5194/bg-10-437-2013,
616 2013.
- 617 McCalley, C.K., Woodcroft, B.J., Hodgkins, S.B., Wehr, R.A., Kim, E-H., Mondav, R., Crill, P.M.,
618 Chanton, J.P., Rich, V.I., Tyson, G.W., and Saleska, S.R.: Methane dynamics
619 regulated by microbial community response to permafrost thaw. *Nature* 514, 478–451,
620 doi:10.1038/nature13798, 2014.
- 621 McFadden, J.P., Eugster, W., and Chapin, F.S., III: A regional study of the controls on water vapor
622 and CO₂ exchange in arctic tundra. *Ecology* 84, 2762–2776, doi:10.1890/01-0444,
623 2003.
- 624 McGuire, A. D., Christensen, T. R., Hayes, D., Heroult, A., Euskirchen, E., Kimball, J. S., Koven,
625 C., Lafleur, P., Miller, P. A., Oechel, W., Peylin, P., Williams, M., and Yi, Y.: An



- 626 assessment of the carbon balance of Arctic tundra: comparisons among observations,
627 process models, and atmospheric inversions, *Biogeosciences*, 9, 3185–3204,
628 <https://doi.org/10.5194/bg-9-3185-2012>, 2012.
- 629 McGuire, A.D., Lawrence, D.M., Koven, C., Clein, J.C., Burke, E., Chen, G., Jafarov, E.,
630 MacDougall, A.H., Marchenko, S., Nicolsky, D., Peng, S., Rinke, A., Ciais, P.,
631 Gouttevin, I., Hayes, D.J., Jin, D., Krinner, G., Moore, J.C., Romanovsky, V.,
632 Schädel, C., Schaefer, K., Schuur, E.A.G., and Zhuang, Q.: Dependence of the
633 evolution of carbon dynamics in the northern permafrost region on the trajectory of
634 climate change, *PNAS* 115.: 3882–3887, doi/10.1073/pnas.1719903115, 2018.
- 635 Mikola, J., Virtanen, T., Linkosalmi, M., Vähä, E., Nyman, J., Postanogova, O., Räsänen, A.,
636 Kotze, D.J., Laurila, T., Juutinen, S., Kondratyev, V., and Aurela, M.: Spatial
637 variation and linkages of soil and vegetation in the Siberian Arctic tundra – coupling
638 field observations with remote sensing data. *Biogeosciences* 15, 2781–2801, 2018.
- 639 Oh, Y., Zhuang, Q., Liu, L., Welp, L.R., Lau, M.C.Y., Onstott, T.C., Medvigy, D., Bruhwiler, L.,
640 Dlugokencky, E.J., Hugelius, G., D’Imperio, L., and Elberling, B. Reduced net
641 methane emissions due to microbial methane oxidation in a warmer Arctic. *Nature*
642 *Climate Change* 10, 317–321, 2020.
- 643 St Pierre, K.A., Kortegaard Danielsen, B., Hermesdorf, L., D’Imperio, L., Lønsmann Iversen, L.,
644 Elberling, B.: Drivers of net methane uptake across Greenlandic dry heath tundra
645 landscapes. *Soil Biology and Biochemistry* 138: 107605,
646 doi.org/10.1016/j.soilbio.2019.107605, 2019.
- 647 Räsänen, A., Manninen, T., Korkiakoski, M., Lohila, A, and Virtanen, T.: Predicting catchment-
648 scale methane fluxes with multi-source remote sensing. *Landscape Ecology* 36, 1177–
649 1195. <https://doi.org/10.1007/s10980-021-01194-x>. 2021.



- 650 Richardson, A.D.: Tracking seasonal rhythms of plants in diverse ecosystems with digital camera
651 imagery. *New Phytologist* 222,1742–1750, doi: 10.1111/nph.15591, 2019.
- 652 Saunois, M., Stavert, A.R., Poulter, B., Bousquet, P., Canadell, J.G., Jackson, R.B., Raymond, P.A.,
653 Dlugokencky, E.J., Houweling, S., Patra, P.K. and Ciais, P.: The global methane
654 budget 2000–2017. *Earth System Science Data*, 12, 1561-1623, 2020.
- 655 Shaver, G.R., Street, L.E., Rastetter, E.B., van Wijk, M.T., and Williams, M.: Functional
656 convergence in regulation of net CO₂ flux in heterogeneous tundra landscapes in
657 Alaska and Sweden. *Journal of Ecology* 95, 802–817, 2007.
- 658 Street, L.E., Shaver, G.R., Williams, M., and van Wijk, M.T.: What is the relationship between
659 changes in canopy leaf area and changes in photosynthetic CO₂ flux in arctic
660 ecosystems? *Journal of Ecology* 95, 139–150, 2007.
- 661 Ter Braak, C.J.F. and Šmilauer, P.: *Canoco reference manual and user's guide: software for*
662 *ordination (version 5.0)*. Microcomputer Power, Ithaca, NY, USA, 2012.
- 663 Treat, C.C., Marushchak, M.E., Voigt, C., Zhang, Y., Tan, Z., Zhuang, Q., Virtanen, T.A., Räsänen,
664 A., Biasi, C., Hugelius, G., Kaverin, D., Miller, P.A., Stendel, M., Romanovsky, V.,
665 Rivkin, F., Martikainen, P.J., and Shurpali, N.J. Tundra landscape heterogeneity, not
666 interannual variability, controls the decadal regional carbon balance in the Western
667 Russian Arctic. *Global Change Biology* 24, 5188–5204, doi: 10.1111/gcb.14421,
668 2018.
- 669 Tuovinen, J-P., Aurela, M., Hatakka, J., Räsänen, A., Virtanen, T., Mikola, J., Ivakhov, V.,
670 Kondratyev, V., and Laurila, T.: Interpreting eddy covariance data from
671 heterogeneous Siberian tundra: land-cover-specific methane fluxes and spatial
672 representativeness. *Biogeosciences* 16, 255–274, doi.org/10.5194/bg-16-255-2019,
673 2019.



- 674 Uttal, T., Starkweather, S., Drummond, J. R., Vihma, T., Makshtas, A. P., Darby, L. S., Burkhart,
675 J. F., Cox, C. J., Schmeisser, L. N., Haiden, T., Maturilli, M., Shupe, M. D., de Boer,
676 G., Saha, A., Grachev, A. A., Crepinsek, S. M., Bruhwiler, L., Goodison, B.,
677 McArthur, B., Walden, V. P., Dlugokencky, E. J., Persson, P. O. G., Lesins, G.,
678 Laurila, T., Ogren, J. A., Stone, R., Long, C. N., Sharma, S., Massling, A., Turner,
679 D. D., Stanitski, D. M., Asmi, E., Aurela, M., Skov, H., Eleftheriadis, K., Virkkula,
680 A., Platt, A., Førland, E. J., Iijima, Y., Nielsen, I. E., Bergin, M. H., Candlish, L.,
681 Zimov, N. S., Zimov, S. A., O'Neill, N. T., Fogal, P. F., Kivi, R., Konopleva-Akish,
682 E. A., Verlinde, J., Kustov, V.Y., Vasel, B., Ivakhov, V.M., Viisanen, Y., and Intrieri,
683 J. M.: International Arctic Systems for Observing the Atmosphere: An International
684 Polar Year Legacy Consortium. *Bull. Am. Meteor. Soc.*, 97, 1033–
685 1056. doi:10.1175/BAMS-D-14-00145.1, 2016.
- 686 Webb, E.E., Schuur, E.A.G., Natali, S.M., Oken, K.L., Bracho, R., Krapek, J.P., Risk, D., and
687 Nickerson, N.R.: Increased wintertime CO₂ loss as a result of sustained tundra
688 warming, *Journal of Geophysical Research Biogeosciences* 121, 249–265,
689 doi:10.1002/2014JG002795, 2016.
- 690 Wickland, K.P., Jorgenson, M.T., Koch, J.C., Kanevskiy, M., and Striegl, R.G.: Carbon dioxide and
691 methane flux in a dynamic Arctic tundra landscape: Decadal-scale impacts of ice
692 wedge degradation and stabilization. *Geophysical Research Letters*, 47,
693 e2020GL089894, doi:10.1029/2020GL089894, 2020.
- 694 van der Molen, M.K., van Huissteden, J., Parmentier, F.J.W., Petrescu, A.M.R., Dolman, A.J.,
695 Maximov, T.C., Kononov, A.V., Karsanaev, S.V., and Suzdalov, D.A.: The growing
696 season greenhouse gas balance of a continental tundra site in the Indigirka lowlands,
697 NE Siberia. *Biogeosciences* 4, 985–1003, doi.org/10.5194/bg-4-985-2007, 2007.



698 Virkkala, A.-M., Virtanen, T., Lehtonen, A., Rinne, J., and Luoto, M.: The current state of CO₂ flux
699 chamber studies in the Arctic tundra: A review. *Progress in Physical Geography*, 42,
700 162–184, 2018.

701 Virkkala, et al.: Statistical upscaling of ecosystem CO₂ fluxes across the terrestrial tundra and
702 boreal domain: regional patterns and uncertainties. *Global Change Biology*,
703 doi:10.1111/GCB.15659, 2021.

704 Virtanen, T. and Ek, M.: The fragmented nature of tundra landscape. *International Journal of*
705 *Applied Earth Observation and Geoinformation* 27, 4–12, 2014.

706 Zhang, W., Jansson, P.-E., Sigsgaard, C., McConnell, A., Manon Jammet, M., Westergaard-Nielsen,
707 A., Lund, M., Friborg, T., Michelsen, A., and Elberling, B.: Model-data fusion to
708 assess year-round CO₂ fluxes for an arctic heath ecosystem in West Greenland
709 (69°N). *Agricultural and Forest Meteorology* 272–273, 176–186, 2019.

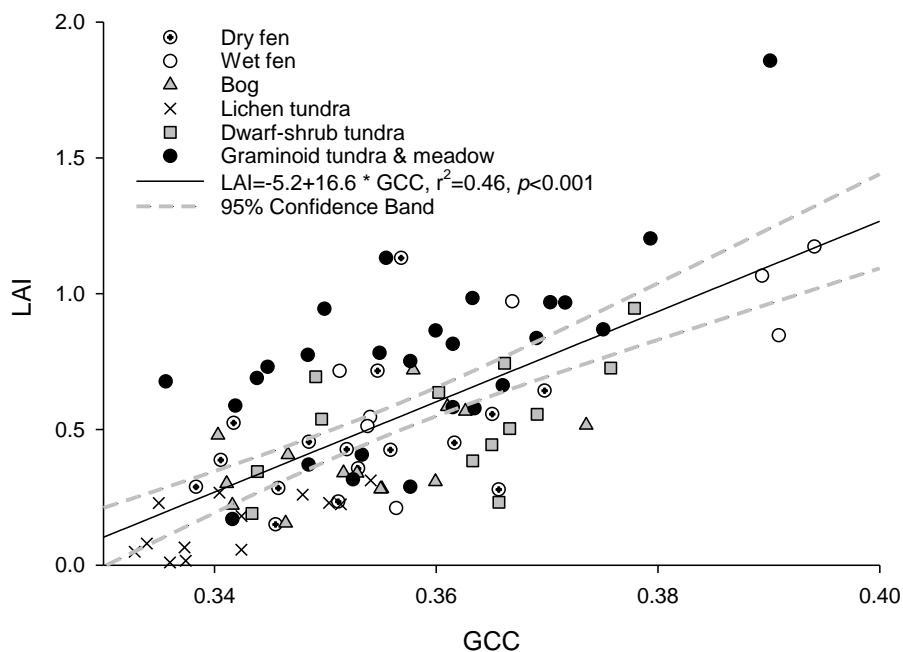
710
711
712
713
714
715
716
717
718
719
720
721
722
723
724
725



726 **Appendix**

727

728



729

730

731

732 Appendix Figure 1. Relationship between GCC and vascular plant LAI in the harvested plots. LCTs
733 are indicated with symbols. In the LCT-specific regressions (not shown), the coefficient of
734 determination ($R^2_{adj.}$) was lowest for dry fen (0.06) and highest for wet fen (0.54). Regression
735 slopes varied from 8.3 for dry fen to 17.8 for the combined graminoid tundra and meadow LC